The Plant Journal (2023) doi: 10.1111/tpj.16273

A complex tissue-specific interplay between the Arabidopsis transcription factors AtMYB68, AtHB23, and AtPHL1 modulates primary and lateral root development and adaptation to salinity

Fiorella Paola Spies[1,†], María Florencia Perotti[1,†], Yuhan Cho[2], Chang Ig Jo[2], Jong Chan Hong[2,3] and Raquel Lía Chan[1,*]

[1]*Instituto de Agrobiotecnología del Litoral, CONICET, Universidad Nacional del Litoral, FBCB, Colectora Ruta Nacional 168 km 0 3000, Santa Fe, Argentina,*

[2]*Division of Life Science, Applied Life Science (BK21 Four), Plant Molecular Biology and Biotechnology Research Center, Gyeongsang National University, Jinju, Gyeongnam 52828, South Korea, and*

[3]*Division of Plant Sciences, University of Missouri, Columbia, South Carolina MO 65211-7310, USA*

Received 18 December 2022; accepted 25 April 2023.
*For correspondence (e-mail rchan@fbcb.unl.edu.ar).
†These authors contributed equally to this work.

SUMMARY

Adaptation to different soil conditions is a well-regulated process vital for plant life. AtHB23 is a homeodomain-leucine zipper I transcription factor (TF) that was previously revealed as crucial for plant survival under salinity conditions. We wondered whether this TF has partners to perform this essential function. Therefore, TF cDNA library screening, yeast two-hybrid, bimolecular fluorescence complementation, and coimmunoprecipitation assays were complemented with expression analyses and phenotypic characterization of silenced, mutant, overexpression, and crossed plants in normal and salinity conditions. We revealed that AtHB23, AtPHL1, and AtMYB68 interact with each other, modulating root development and the salinity response. The encoding genes are coexpressed in specific root tissues and at specific developmental stages. In normal conditions, *amiR68* silenced plants have fewer initiated roots, the opposite phenotype to that shown by *amiR23* plants. AtMYB68 and AtPHL1 play opposite roles in lateral root elongation. Under salinity conditions, where AtHB23 plays a crucial positive role, AtMYB68 cooperates with AtHB23, whereas AtPHL1 obstructs its action, impacting the plant's survival ability and supporting the complex interaction between AtHB23, AtPHL1, and AtMYB68 in primary and lateral roots. The root adaptation capability is associated with the amyloplast state. We identified new molecular players that through a complex relationship determine Arabidopsis root architecture and survival in salinity conditions.

Keywords: root development, AtHB23, AtMYB68, AtPHL1, salinity, protein–protein interaction.

INTRODUCTION

Plants' adaptation to the environment is a finely regulated process involving different biomolecules and levels of modulation. Roots are the anchorage organs that firstly sense changes in the soil and accordingly accelerate or arrest their primary or lateral growth and development for better adaptation, optimizing water and nutrient uptake (de Dorlodot et al., 2007; Waidmann et al., 2020). They enable plant adaptation to unfavorable environments by integrating different cues and balancing growth and development (Schachtman & Goodger, 2008).

Phytohormones like ABA and auxin play crucial roles in such adaptation. Under salinity stress, the growth of the primary root is inhibited concomitantly with a decrease in the auxin content in the tip. Auxin transport toward roots is carried out in the central cylinder by AUX1, LAX1, LAX2, and LAX3 carriers exhibiting specific expression patterns impacting the phytohormone content in each tissue (Friml et al., 2003; Péret et al., 2012; Swarup & Péret, 2012). In the tip, NaCl regulates AUX1 and PIN2 (Liu et al., 2015). Low NaCl concentrations (≤50 mM) generate lateral root (LR) growth, whereas higher NaCl concentrations repress it, and these changes depend on auxin transport and distribution (Zolla et al., 2010).

Salinity stress and auxin content and distribution are closely related. Starch granule synthesis happens in the columella cells, and this process is influenced by salinity,

affecting the gravitational response (Korver et al., 2020; Leitz et al., 2009; Zhang et al., 2019).

Molecular events modulating root architecture and plasticity in changing and harmful conditions involve the participation of transcription factors (TFs). These regulatory proteins play crucial roles, usually activating or repressing entire transcriptional programs. Plants' TFs are abundant (about 1600 in Arabidopsis and 1500 in rice [*Oryza sativa*]) and are classified into families and subfamilies, mainly according to their DNA binding domains, which determine their target specificity (González, 2016; Hong, 2016). For example, in LR development, proteins from the Auxin Response Factor (ARF) and Lateral Organ Boundaries Domain (LBD) families have been described as master regulators (Banda et al., 2019; Friml et al., 2003; Lavenus et al., 2013; Lee et al., 2009; Xu et al., 2020).

The homeodomain (HD) TF family is large; its members differ in size, gene structure, localization of the HD, and other features (Capella et al., 2016). This fact generated a further classification of subfamilies. Among them, the HD-Zip subfamily is composed of proteins having a leucine zipper (LZ) domain downstream of and adjacent to the HD and divided into four groups (I to IV). Functional divergence between members of subfamily I, and neofunctionalization, was explained by different uncharacterized motifs in the N- and C-termini of such proteins (Arce et al., 2011; Capella et al., 2014). Among these motifs, the AHA motif, at the C-terminus, interacts with the basal transcriptional machinery (Capella et al., 2014). However, deletion of the AHA motif to avoid transactivation in yeast two-hybrid (Y2H) assays indicated that the proteins still interact with others. Such was the case of AtHB23 (AtHB23ΔAHA), used as bait to screen an Arabidopsis TF library, which revealed the interaction with four different proteins (Spies et al., 2022), including three belonging to the large MYB family, AtMYB68 (At5g65890), AtPHL1 (At5g29000), and AtMYB12 (At2g47460), and AtWRKY43 (At2g46130; Spies et al., 2022).

AtHB23 is a member of group α (Henriksson et al., 2005) or clade V (Arce et al., 2011). *AtHB23* is expressed in the LR primordium (LRP), acting as a negative regulator of LR initiation, and in the tip of primary roots involved in the salinity response (Perotti et al., 2019). It is directly regulated by ARF7/19, and *LAX3* and *LBD16* are its targets (Perotti et al., 2019, 2022).

AtMYB68 is expressed during LR development and transcriptionally induced by high temperatures (Feng et al., 2004). However, its role in LR development remains uncertain. It is involved in several regulatory networks controlling development, metabolism, and the responses to biotic and abiotic stresses (Dubos et al., 2010). A few members of this family, such as AtMYB52, AtMYB53, AtMYB56, and AtMYB87, have been linked to LR development. Moreover, they participate in the intricate auxin-responsive network of TFs (Lavenus et al., 2015).

AtPHL1 belongs to the 15-member MYB-CC subfamily, which is characterized by the presence of a MYB domain and a coiled-coiled (CC) domain (Rubio et al., 2001). Although AtPHL1 was thought redundant with AtPHR1, the most-studied protein of this family, such redundancy was only partial and related to Pi starvation. PHR1 was identified as the master modulator of Pi deficiency responses, inducing transcription of Pi starvation genes, whereas the aberrant expression of *phl1* was only mildly affected, indicating a minor role in such event (Bustos et al., 2010). Analysis of the double mutant *phr1*/*phl1* revealed that both genes participate in iron homeostasis regulation (Bournier et al., 2013). Besides their participation as players in the Pi starvation response in several plant species, the role of MYB-CC TFs in root development or stress responses remains largely unknown.

It was previously reported that *AtPHL1* and *AtHB23* are coexpressed in the pedicel–silique nodes and the funiculus, interacting to promote sucrose transport (Spies et al., 2022). In the present work, we investigated the interplay between AtHB23, AtMYB68, and AtPHL1 and their role in root development. We found that AtHB23 interacts with both MYB TFs in yeast and in plants. Moreover, these MYB TFs interacted with each other as well. The three TFs are coexpressed in specific cell groups and during specific developmental stages of the primary roots and LRs. Under control and salinity conditions, they play cooperative and opposite roles depending on the situation.

RESULTS

The interaction between transcription factors AtHB23, AtPHL1, and AtMYB68 was validated in yeast, *in vitro*, and *in planta*

HD-LZ TFs harbor uncharacterized motifs at their N- and C-termini, potentially interacting with other specific proteins (Arce et al., 2011). Such was the case of AtHB23, used as bait to screen an Arabidopsis TF library, allowing the identification of four putative partners. In previous work, we corroborated the interaction between AtHB23 and AtPHR1-like1 (hereafter, AtPHL1) by carrying out independent Y2H and bimolecular fluorescence complementation (BiFC) assays (Spies et al., 2022). Moreover, the functional meaning of such an interaction was studied in conductive tissues and siliques (Spies et al., 2022), whereas the interaction with AtMYB68 (At5g65890) remained unexplored. Hence, we decided to continue the study with this putative AtHB23 partner.

Firstly, we verified the interaction between AtHB23 and AtMYB68 by independent Y2H and β-galactosidase activity assays (Figure 1a). To further validate the relationship *in planta*, we examined their subcellular localization and determined that they colocalized in the nucleus (Figure 1b). Moreover, their interaction was confirmed by

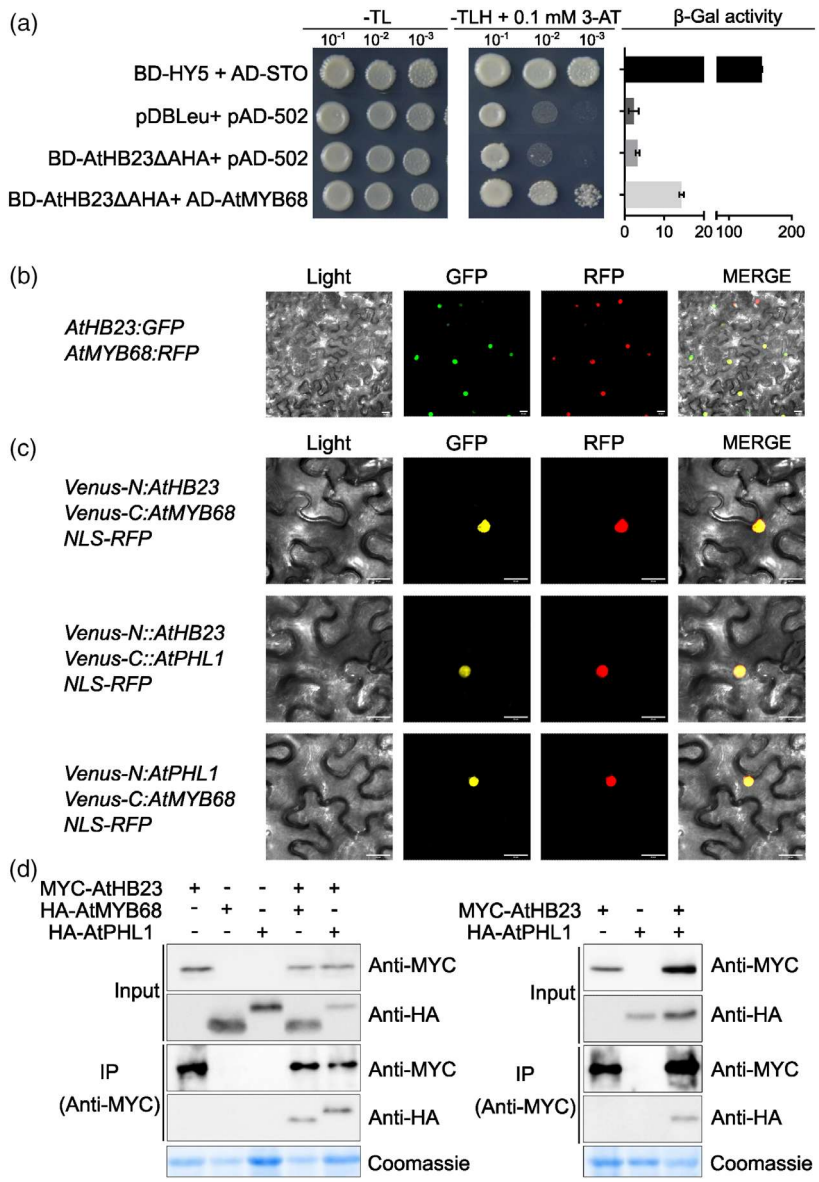

Color 11

Figure 1. The transcription factors AtHB23, MYB68, and PHL1 interact with each other in yeast and *in planta*.
(a) Y2H assay performed with BD-AtHB23ΔAHA + AD-MYB68 and the corresponding controls on selection media (SD−Trp,Leu [−TL], SD−Trp,Leu,His [−TLH], and −TLH with 0.1 mM 3-amino-1,2,4-triazole[−TLH+3-AT]). On the right panel, β-galactosidase activity in miller units is shown. BD, Gal4 DNA binding domain; AD, Gal4 activation domain. BD-HY5 + AD-STO and pDBLeu + pAD-502 were used as positive and negative controls, respectively. In AtHB23ΔAHA, the C-terminal AHA domain was removed (Capella et al., 2014). (b) Colocalization assay using *Nicotiana benthamiana* leaves. *Agrobacterium tumefaciens* harboring *35S:AtHB23:GFP* and *35S:AtMYB68:RFP* were infiltrated and pictures were taken 2 days after with a confocal microscope. GFP, GFP image; RFP, RFP image; Merge, merge of fluorescence and light images. (c) Mutual interactions between AtHB23, AtMYB68, and AtPHL1 *in planta*. *Agrobacterium tumefaciens* transformed with *N-YFP:AtHB23* and *C-YFP:AtMYB68*, with *N-YFP:AtHB23* and *C-YFP:AtPHL1*, with *N-YFP:AtPHL1*, and with *C-YFP:AtMYB68* were used. NLS-RFP was used for cotransformation as a nuclear localization signal. (d) Coimmunoprecipitation assay *in vivo*. AtHB23 carrying a Myc tag (MYBC-HB23) was coexpressed with HA-tagged AtMYB68 (HA-AtMYB68) and AtPHL1 (HA-AtPHL1). The right panel shows the interaction between Myc-AtHB23 and HA-AtPHL1.

BiFC assays in *Nicotiana benthamiana* leaves (Figure 1c; Figure S1).

Given that the established relationships were independent, AtHB23 with AtMYB68 or with AtPHL1, we wondered whether AtMYB68 and AtPHL1 also interacted with each other. Unfortunately, Y2H analysis between Gal4BD-AtHB68 and Gal4BD-AtPHL1 did not succeed because Gal4BD-AtMYB68 and Gal4BD-AtPHL1 showed strong transcription activities in yeast. Therefore, we performed a BiFC assay using VENUS-N:AtPHL1 and VENUS-C:AtMYB68 with positive results (Figure 1c; Figure S1). Furthermore, these proteins colocalized in the nucleus when tobacco leaves were cotransformed (Figure 1c). A reciprocal combination of the three TFs constructed in the N-VENUS and C-VENUS vector

sets resulted in crossed interactions with each other (Figure S1). Next, we performed coimmunoprecipitation assays to confirm the obtained results by an independent method (Figure 1d). Total protein extracts from tobacco plants transiently transformed with Myc-AtHB23 plus HA-AtMYB68 and Myc-AtHB23 plus HA-AtPHL1 were pulled down with anti-Myc antibodies (Figure 1d, left panel). Both pairs coimmunoprecipitated, supporting the above described results (Figure 1d, right panel).

AtMYB68 and *AtPHL1* are coexpressed with *AtHB23* in specific tissues and during specific developmental stages of root development

To test the functional role of the interaction between these three TFs, we first investigated the expression patterns of *AtMYB68* and *AtPHL1* in roots, the organ in which *AtHB23* was deeply investigated, associated with developmental and salinity responses (Perotti et al., 2019, 2020, 2022). For this purpose, we used 8-day-old transgenic plants carrying the constructs *prAtMYB68:GUS* and *prAtPHL1:GUS*. *AtPHL1* was expressed in the root tip and at the base of the LRP in stages V to VII (Malamy & Benfey, 1997) and in the tip of emerged LRs. GUS activity driven by the *AtMYB68* promoter was evident in vascular tissue and in developing LRPs and LRs (Figure 2; Figure S2). *AtMYB68* and *AtPHL1* coincided with *AtHB23* at the base of LRPs, hinting at a coordinated role of these interacting TFs in LR development (Figure S3). Later, *AtMYB68* expression in LR development was restricted to the surrounding cells of the primordium, resembling that of other auxin-responsive genes involved in this developmental context (Figure 2; Marin et al., 2010).

AtMYB68 and AtPHL1 play a role in primary and lateral root development together with AtHB23

Given the expression patterns and interactions described above, we wondered whether regulation at the transcriptional level between these genes takes place in specific root tissues. To elucidate this question, we obtained *AtMYB68* silenced (*amiR68*; no mutants were available in the Col-0 background) and *AtMYB68* overexpression (AT68) plants with altered transcript levels (Figure S4). Transcript levels of *AtHB23*, *AtPHL1*, and *AtMYB68* were evaluated in *amiR23*, *phl1*, *amiR68*, AT23, ATPHL1, and AT68 genotypes (Figure S5). Notably, except for *AtMYB68*, showing very mild downregulation in *phl1* and *amiR23* roots, the transcript levels were not altered, either in mutants or in overexpression plants, indicating that the contribution to transcriptional regulation is not relevant in this case.

Considering the tissue-specific and subcellular colocalization of AtMYB68, AtPHL1, and AtHB23, plus their interaction in yeast and *in planta*, we investigated how these genes affect root architecture. The number of initiated and emerged LRs in *amiR68* plants and *phl1* mutants was evaluated. *AtMYB68* silencing did not affect primary root length but significantly reduced the LRP density (Figure 3a), the opposite phenotype to that of *amiR23* plants (Perotti et al., 2019). *Phl1* mutants and *amiR23* plants had longer primary roots, whereas *PHL1* overexpressors (ATPHL1) showed the opposite phenotype (Figure 3c). On the other hand, *phl1* mutants did not exhibit significant differences in the number of LRPs or LRs. *AtMYB68* overexpressors showed a similar phenotype (Figure S6).

Remarkably, relative total LR length was diminished in *amiR68* plants and significantly augmented in *phl1* mutants, like in *amiR23* plants (Figure 3b). To test whether LRs differed between the three genotypes in cell number or cell size, LR root tips were analyzed by confocal microscopy. The analysis revealed fewer cells in *amiR68* plants in the transition zone, whereas *phl1* and *amiR23* mutant plants showed the opposite phenotype (Figure 3d,e).

Altogether, the results indicate a complex interplay between the three partners at the base of the LRP and the LR tip.

Auxin induces *AtMYB68* expression impacting the hormone distribution in the root

Given that *AtHB23* expression in LRs is regulated by auxin and the encoded protein directly modulates the gene

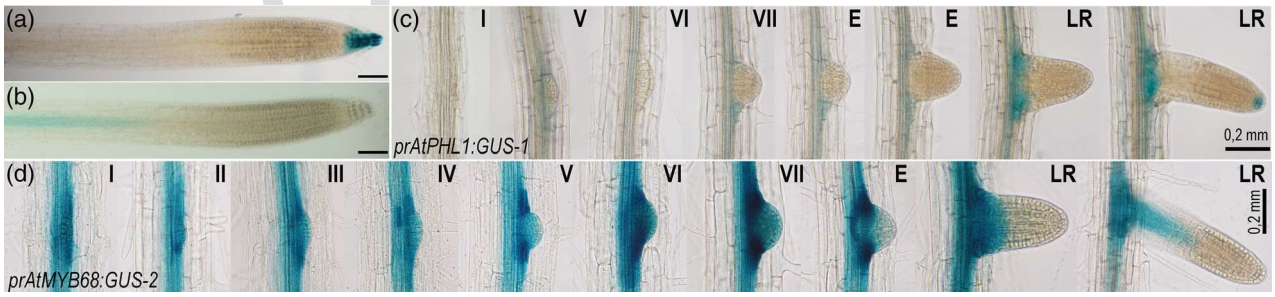

Figure 2. *AtMYB68* and *AtPHL1* genes are expressed in primary and lateral roots.
(a, b) Expression of *AtPHL1* (a) and *AtMYB68* (b) in the primary root, evaluated with *prAtPHL1:GUS* and *prAtMYB68:GUS* transgenic plants. (c, d) Expression pattern of the same genes during lateral root development. I to VII represent different stages of lateral root primordium (LRP) development; LR indicates emerged roots as described by Malamy and Benfey (1997). The black bar indicates 50 μm.

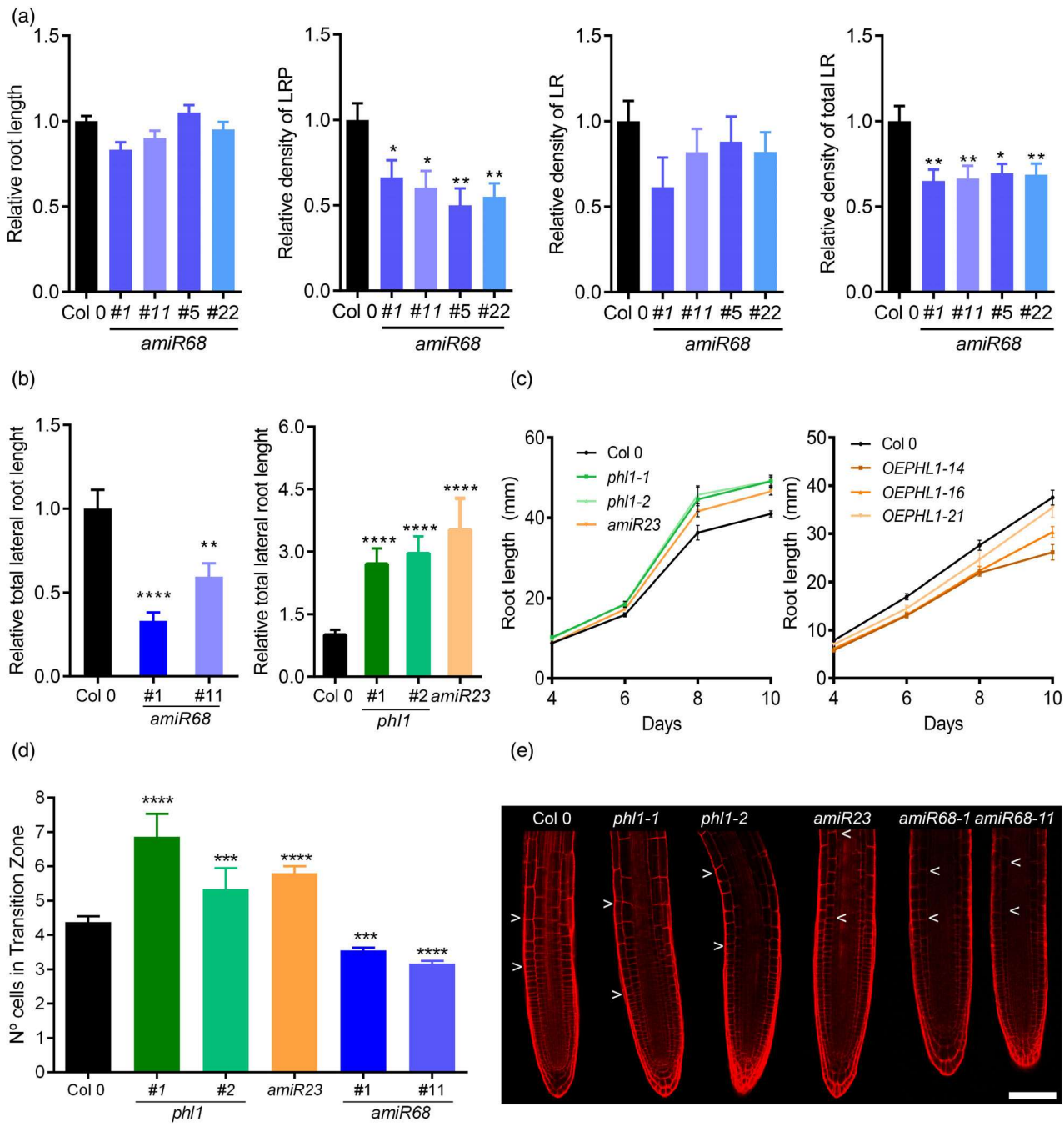

Color

Figure 3. *AtMYB68* and *AtPHL1* modulate root architecture.
(a) Relative main root length in 8-day-old *amiR68* mutants compared with the Col-0 control. The relative density of LRPs or LRs was calculated as the number of LRPs or LRs per mm of the primary root, and the relative density of total lateral roots (LRPs + LRs) was also calculated. The values were normalized to those in the control Col-0. For root length, 100% = 18.27 mm; for LRP density, 100% = 0.64 LRPs mm^{-1}; for LR density, 100% = 0.25 LRs mm^{-1}; and for total RL density, 100% = 0.88 LRs mm^{-1}. (b) Total LR length of Col-0 and *amiR68*, *phl1*, and *amiR23* mutants. In the left panel, 100% = 13.03 mm, and in the right panel, 100% = 0.67. (c) Time course of root elongation of *phl1* and OEPHL1 relative to Col-0 plants; 100% = 8.78, 15.85, 36.27, and 40.97 mm (left panel) and 100% = 7.85, 16.95, 27.58, and 37.52 mm (right panel). (d) Number of cells in the transition zone of Col-0, *amiR68*, *phl1*, and *amiR23* mutants. (e) Illustrative confocal microscopy picture of root tips of Col-0 and *amiR68*, *phl1*, and *amiR23* mutants. Assays were repeated three times with $n = 15$ per genotype. Error bars represent SEM. Asterisks indicate significant differences as determined using Student's *t*-test (**$P < 0.01$, ***$P < 0.001$, ****$P < 0.0001$).

expression of the auxin carrier LAX3, we wondered whether its partners were also regulated by this hormone. *PrMYB68:GUS* plants were treated with 1 μM IAA and analyzed by histochemistry and reverse transcriptase quantitative PCR (RT-qPCR). Both assays indicated a strong induction of this gene by auxin in the root vascular system

(Figure 4a,b). We also tested the effect of auxin on the expression in the root tip of *AtPHL1* and *AtHB23*. *AtPHL1* did not exhibit significant differences in the presence of IAA, whereas *AtHB23* showed strong induction in the vascular system (Figure S7). In view of the impact of IAA on *AtMYB68*, we used *DR5:GUS* plants to cross them with *amiR68* mutants. Notably, *DR5* expression in the primary root tip disappeared in the crosses, indicating repression of the hormone transport to this tissue. The effect was similar in LR tips, whereas DR5 staining increased in the LRPs (Figure 4c,d). To elucidate the influence of AtPHL1, we generated new crosses between *DR5:GUS* and *phl1* mutants. In this case, the expression in the tips remained unaltered, whereas it disappeared from the vascular system (Figure 4e). Regarding auxin carriers, AUX1 appeared strongly induced by AtMYB68 because the crosses *prAUX1:GUS* × *amiR68* showed significantly less staining than *prAUX1:GUS* plants (Figures 4f,g).

AtMYB68 and AtPHL1 play opposite roles under salinity conditions

Considering the impact of the interaction between AtMYB68, AtPHL1, and AtHB23 in root architecture and given the positive role of AtHB23 in salinity conditions, we wondered whether these MYB TFs were necessary for such a response. To answer this question, we analyzed the expression of these genes in salinity conditions. Transgenic plants carrying *prAtMYB68:GUS* and *prAtPHL1:GUS*

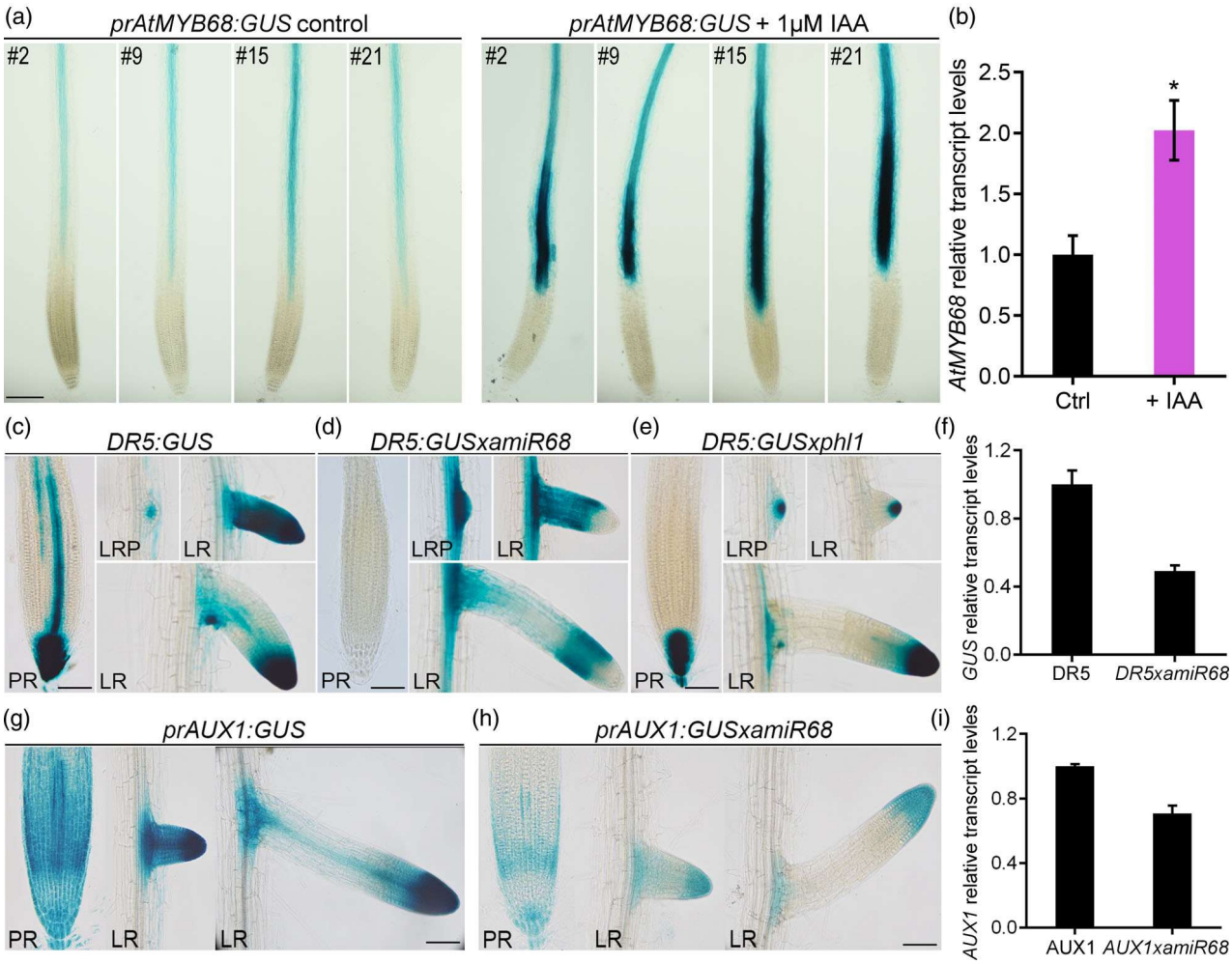

Figure 4. *AtMYB68* expression is induced by IAA and alters auxin distribution.
(a) GUS histochemistry of 8-day-old *prAtMYB68:GUS* roots (four independent lines: *#2, #9, #15,* and *#21*) grown in control conditions (left panel) or treated with 1 µM IAA (right panel) for 12 h. The black bar indicates 50 µm. (b) Transcript levels of *AtMYB68* in 7-day-old roots of seedlings grown in standard conditions or with 1 µM IAA for 12 h. The value was normalized to that in the control Col-0. (c–e) GUS histochemistry of 8-day-old *DR5:GUS* (c), *DR5:GUS* × *amiR68* (d), and *DR5:GUS* × *phl1* (e) roots. (f) Transcript levels of *GUS* in 8-day-old *DR5:GUS* and *DR5:GUS* × *amiR68* roots of seedlings. The values were normalized to the control *DR5:GUS*. (g, h) *prAUX1:GUS* and *prAUX1:GUS* × *amiR68* roots. (i) Transcript levels of *GUS* in 8-day-old *prAUX1:GUS* and *prAUX1:GUS* × *amiR68* roots. Value were normalized to the control *prAUX1:GUS*. Asterisks indicate significant differences (post hoc Tukey test). PR, primary root; LRP, lateral root primordium; LR, emerged lateral roots. The black bar indicates 50 µm. Assays were repeated three times with n = 15 per genotype.

The Plant Journal, (2023), doi: 10.1111/tpj.16273

were subjected to NaCl treatment and analyzed by histochemistry. *AtPHL1* was strongly induced in the root tip and the vascular system (Figure 5a), whereas *prAtMYB68:GUS* plants did not exhibit significant differences in GUS staining. However, *AtMYB68* transcript levels were significantly increased in Col-0 plants treated with NaCl (Figure 5b). To test whether the modulation of the expression of these genes by NaCl impacts mutant and overexpressor phenotypes, we counted survivors and dead plants after 9–15 days of treatment; *amiR68* and ATPHL1 plants showed similar sensitive phenotypes (Figure 5c). Moreover, ATPHL1 plants arrested the growth of the primary root, whereas *phl1* mutants showed the opposite behavior (Figure 5d). Considering total LR length, these mutants treated with NaCl resembled the Col-0 genotype, whereas *amiR68* and *amiR23* seedlings, which in normal conditions exhibited shorter LRs, were less sensitive than the Col-0 under salinity considering this trait (Figure 5e).

The adaptation ability of *AtHB23, AtPHL1*, and *AtMYB68* mutants, overexpressors, and crossed plants to salinity is correlated with the starch granule state in the root tip

Root gravitropism depends on the auxin gradient between the upper and lower sides (Zhang et al., 2019). In the columella cells, starch aggregates are formed, named statoliths or amyloplasts (Leitz et al., 2009). A saline medium severely affects the auxin gradient and consequently amyloplast formation. *AtHB23*, *AtPHL1*, and *AtMYB68* mutant and overexpressor plants differentially responded to salinity stress (Figure 5). To understand this, we analyzed starch content by staining the root tips of these plants with Lugol solution (Figure 6). Seedlings were grown in normal conditions for 5 days (Figure 6a) and then placed in 150 mM NaCl for 7–8 h (Figure 6b). It was previously shown that *amiR23* plants significantly reduced their starch content after this treatment (Perotti et al., 2022; Figure 6b). As expected, *amiR68* and

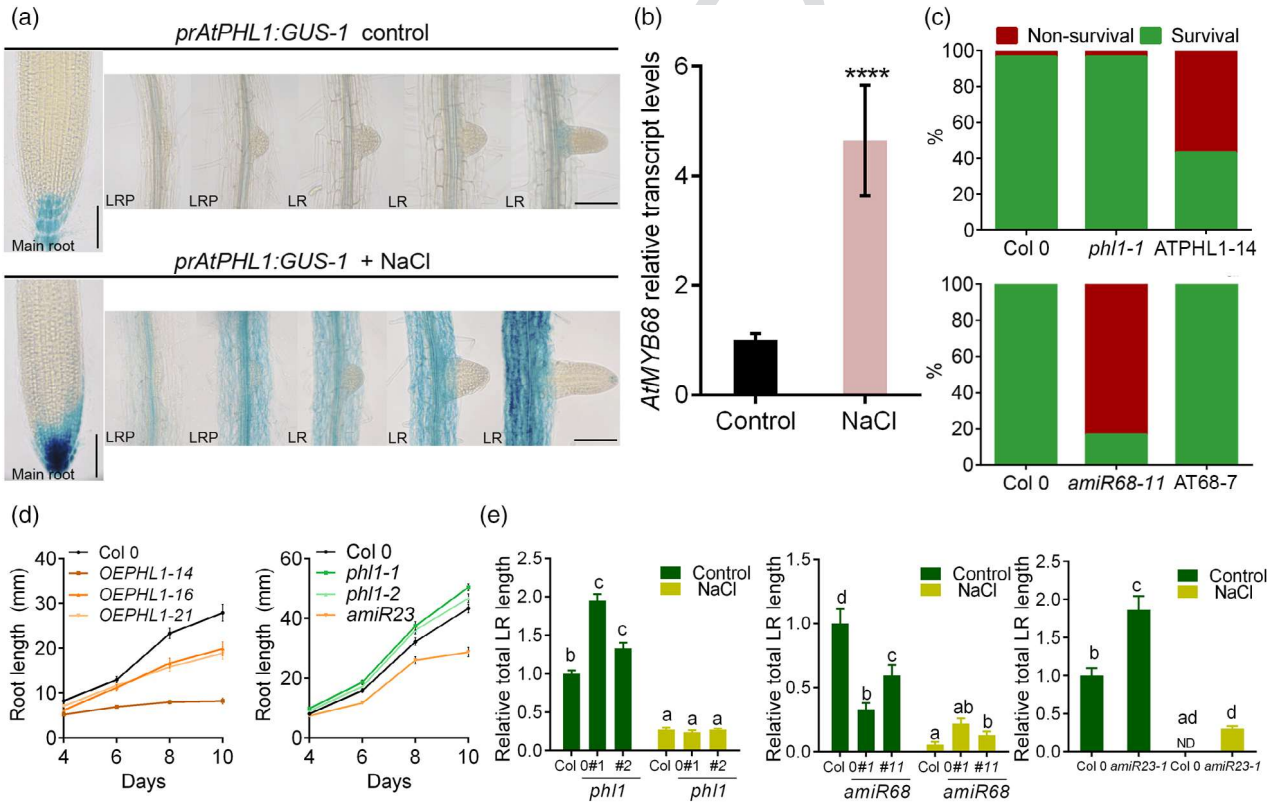

Color

Figure 5. AtMYB68 has a positive role in the response to salinity, whereas AtPHL1 is a negative regulator of such response.
(a) GUS histochemistry of 8-day-old *prAtPHL1:GUS-1* roots (upper panel) and after treatment with 100 mM NaCl (lower panel). (b) Transcript levels of *AtMYB68* in 7-day-old roots of seedlings grown in standard conditions or with 100 mM NaCl for 12 h. Values were normalized to the Col-0 control. The asterisk indicates a significant difference (post hoc Tukey test). (c) Survival rate of Col-0, *phl1*, ATPHL1, *amiR68*, and AT68 plants placed in plates with 100 mM NaCl 3 days after sowing for 9–15 additional days. Red columns indicate the percentage of dead plants and green columns indicate the percentage of survivors. (d) Time course of the main root length evaluated in Col-0, OEPHL1 (three independent lines: *#14, #16*, and *#21*), *phl1* (two independent lines: #1 and #2) mutant, and *amiR23* seedlings grown in 75 mM NaCl. Quantitative measurements were performed from day 4 after sowing until day 10. (e) Total LR length of Col-0, *phl1*, *amiR68*, and *amiR23* mutants grown in control conditions or treated with 75 mM NaCl. In the left panel, 100% = 8.63 mm; in the middle panel, 100% = 13.03 mm; and in the right panel, 100% = 7.66 mm.
The assays were repeated at least three times with $n = 15$ per genotype. The black bar represents 1 cm. Different letters indicate significant differences (Tukey test, $P < 0.01$). Error bars represent SEM.

ATPHL1 genotypes exhibited the same phenotype (Figure 6b). The phenotype of *amiR68* seedlings was rescued in plants crossed with the AT68 genotype, indicating that the silencing of this gene was responsible for the NaCl-enhanced sensitivity (Figure 6b). Afterward, one half of the seedlings were transferred back to MS medium while the other half remained in NaCl. Like AT23 plants, *phl1* and AT68 roots slowly adapted to the saline medium and

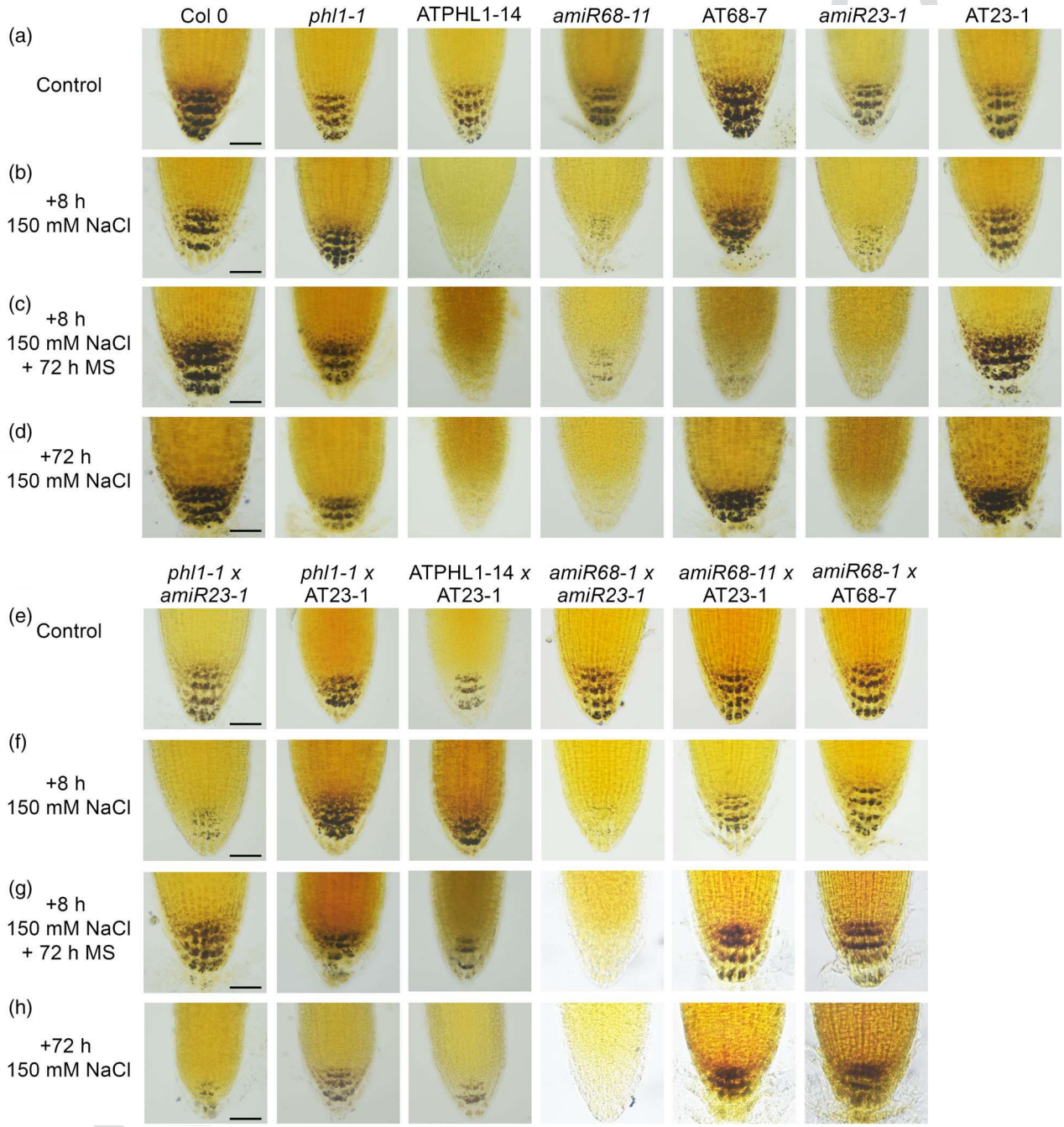

Color

Figure 6. The adaptation ability to salinity conditions depending on *AtHB23*, *AtPHL1*, and *AtMYB68* levels is correlated with the starch granule stage in the root tip.

(a) Illustrative pictures of 5-day-old root tips of Col-0, *phl1*, OEPHL1, *amiR68*, AT68, *amiR23*, and AT23 seedlings grown in normal conditions stained with Lugol solution. (b) After 8 h of treatment with 150 mM NaCl. (c, d) The roots were transferred to normal conditions (c) or maintained in 150 mM NaCl for an additional 72 h (d). (e–h) The same analysis was carried out with the crosses *phl1* × *amiR23*, *phl1* × AT23, OEPHL1 × AT23, *amiR68* × *amiR23*, and *amiR68* × AT23. (e) Control conditions. (f) After 8 h in 150 mM NaCl. (g) After 8 h in 150 mM NaCl + 72 h in MS medium. (h) After 8 h + 72 h in 150 mM NaCl. The black bar represents 50 μm.

The Plant Journal, (2023), doi: 10.1111/tpj.16273

recovered their starch granules as they did in the NaCl-free medium (Figure 6c,d), whereas *amiR68* and ATPHL1 genotypes were unable to restore a healthy phenotype (Figure 6c,d; Figure S8).

Salinity and osmotic stresses are closely related. Moreover, plant transfer from the control condition to medium containing 150 mM NaCl can cause an osmotic shock. To corroborate or discard that the phenotypes observed in mutants and overexpressors were due to salinity and/or osmotic stress, we analyzed starch amyloplasts after treatment with 150 mM mannitol (Figure S9).

None of the genotypes with altered levels of AtHB23, AtPHL1, or AtMYB58 was affected by this treatment, indicating that the observed effects were salinity-specific.

Given these results, we stated the hypothesis based on the availability of AtHB23 to exert a positive action dealing with salinity, avoided by AtPHL1 or enhanced by AtMYB68. To test this, we obtained crossed plants and assayed their behavior by performing the same assay described above. *amiR23* × *amiR68* plants lost their amyloplasts and could not recover them after 72 h in normal conditions (Figure 6e–h). Notably, *amiR68* × AT23 plants did not lose their starch granules after the NaCl treatment, suggesting that the overexpression of *AtHB23* compensated somehow for the low availability of AtMYB68 to cooperatively interact. On the other hand, *phl1-1* × *amiR23* seedlings behaved like the *amiR23* genotype, supporting the essential role of AtHB23 in the positive response to salinity. In ATPHL1 × AT23 crosses, the picture was intermediate between that of the parent genotypes (Figure 6e–h).

Regarding these results, we evaluated transcript levels of genes encoding key enzymes participating in starch synthesis and degradation in *phl1* and *amiR68* plants. The transcript levels of *ADG1* and *PGM*, which are involved in starch synthesis, did not significantly change, except in *amiR68* roots, where they were slightly reduced in salinity conditions and after recovery, respectively (Figure S10). The gene expression of *BAM1*, participating in degradation, was induced in *amiR68* plants in salinity conditions, whereas *phl1* mutants behaved similarly to the WT and GWD did not show differences. These results indicate that starch turnover was altered by the levels of *AtMYB68* and *AtPHL1* (Figure S10). However, they alone cannot explain the absolute lack of starch observed in *amiR68* plants and the amyloplast integrity in *phl1* mutants, indicating that other mechanisms must also be modulating this process.

DISCUSSION

Root plasticity is crucial for plant adaptation to different soil conditions and involves the growth or arrest of the primary, lateral, and high-order roots. These events are finely modulated by many biomolecules, such as TFs and phytohormones. Many detailed studies reported the functional characterization of TFs in LR initiation, emergence, and elongation, as well as in primary root growth (Banda et al., 2019). These studies were performed in normal growth conditions and under different stress factors (Ambastha et al., 2020; Verma et al., 2022). However, information on the involvement of individual TFs in the determination of global architecture, including primary roots and LRs, is less abundant. Here, we reported how three TFs, one HD-Zip TF and two MYB family members, interact to activate or repress primary root and LR development, depending on the environmental conditions. 18

AtHB23, the most-studied protein among the three, was shown to be non-redundant with its putative paralog AtHB13 in roots (Perotti et al., 2019). AtPHL1 was studied only with respect to its secondary role compared with its paralog AtPHR1 in the Pi starvation response (Bustos et al., 2010). 19 *AtMYB68* is expressed in the root pericycle of the Ler ecotype, responding to environmental cues (Feng et al., 2004), and is also detected in the Arabidopsis root protein expression landscape (Petricka et al., 2012). Its role in the reproductive stage was also studied, and it was found to affect seed yield and tolerance to drought and high temperatures (Deng et al., 2020). 20

Several members of the HD-Zip I family are expressed in different root tissues (Perotti et al., 2021), and a few were 21 functionally characterized as being involved in root development and the response to stress (Miao et al., 2018; Mora et al., 2022). MYB-CC proteins were studied in several species, and were found to be particularly associated with the Pi starvation response (Bai et al., 2019; Bhutia et al., 2020). 22 The large MYB family has many well-characterized members acting in roots. For example, AtMYB77 was shown to regulate a subset of auxin-responsive genes during LR development and interacted *in vitro* with ARF proteins. The knockout mutant *atmyb77* exhibits a lower density of LRs than the WT (Shin et al., 2007). Also, AtMYB93 is an auxin-inducible gene acting as a negative regulator of LR development in Arabidopsis, being part of an auxin-triggered negative feedback loop, ensuring that LRs only develop when required (Gibbs et al., 2014). Finally, AtMYB36 was reported as a regulator of the transition from proliferation to differentiation in the endodermis. The characterization of *atmyb36* mutants suggested that this TF acts as a positive regulator of differentiation and a negative regulator of proliferation in root meristems (Liberman et al., 2015).

Although there are significant differences in root development depending on the ecotype (Perotti et al., 2020), the 23 expression pattern reported in Ler plants (Feng et al., 2012) was similar to the one described in the present manuscript.

There is abundant literature about the transcriptional, post-transcriptional, and post-translational regulation of TFs, influencing their stability or activity (Deribe et al., 2010; Nelson & Millar, 2015; Zhang et al., 2021; Zhu, 2016). However, it is hard to find literature describing TFs functioning in both primary root and LR development and also about the association between members of different families acting

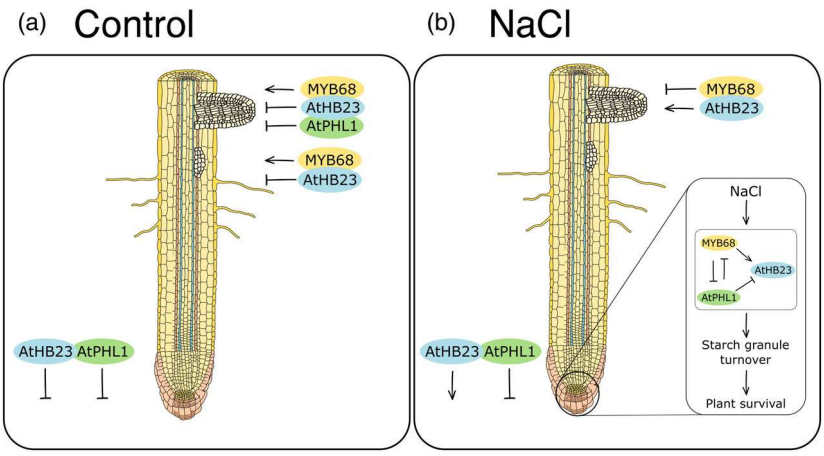

Figure 7. Proposed model for the interactive action of AtHB23, AtPHL1, and AtMYB68 in normal and salinity conditions.
(a, b) Proposed model for the roles of AtHB23, AtPHL1, and AtMYB68 in primary and lateral root development in control (a) and salinity (b) conditions. Arrows between actors indicate direct regulation.

cooperatively or in opposite ways by protein–protein associations. TF partitioning between the nucleus and the cytoplasm is an essential mechanism regulating developmental events and adaptation (Allen & Strader, 2021). Such is the case of the interaction between the HD-Zip I TF HaHB11 from *Helianthus annuus* and AtHB7 from Arabidopsis, modulated by Kinesin13B (Miguel et al., 2020). Despite this scarcity, it was recently reported that the OsFTIP6–OsHB22–OsMYBR57 module regulates drought tolerance in rice (Yang et al., 2022). Notably, OsHB22 is an HD-Zip I TF previously reported as a negative regulator in ABA-mediated drought and salt tolerance in rice (Zhang et al., 2012). Rice mutants in this gene behaved better under drought stress, showing no yield penalty (Zhang et al., 2012). OsMYBR57 is a MYB-related protein; its mutant displayed a drought-sensitive phenotype. Yang et al. (2022) revealed that it interacts with the HD-Zip OsHB22 and both TFs together modulate the expression of several bZIP TFs participating in the drought response. Another example is the interaction in the nucleus between XPO1-interacting WD40 protein 1 (XIW1) and ABA INSENSITIVE 5 (ABI5), modulating the ABA response (Xu et al., 2019).

Coexpression of TFs in the same tissue, during the same developmental stage, and under the same environmental conditions is an absolute requirement for interaction. We showed that *AtHB23*, *AtMYB68*, and *AtPHL1* are expressed in the primary root tip and during specific stages of LR development (Figure 2). Remarkably, *amiR68* mutants exhibited fewer LRPs, the opposite phenotype of *amiR23* plants (this paper and Perotti et al., 2019), suggesting that AtHB23 needs AtMYB68 to exert its function. AtPHL1 does not participate in LR initiation (Figure S6) but it does participate in LR elongation, having a cooperative role with AtHB23, opposing that of AtMYB68, at least in normal conditions (Figure 3). Regarding primary root growth, AtMYB68 seems absent, whereas AtPHL1 and AtHB23 exhibit opposite roles (Figure 3).

AtMYB68 was induced by auxin in the vascular system. Although we could not detect its expression in the root tip of *prAtMYB68:GUS* seedlings, it seriously affected auxin distribution in this tissue, as shown by the *DR5:GUS* × *amiR68* cross (Figure 4). AtPHL1 did not affect auxin levels in the tips of primary roots and LRs, but it did affect auxin levels in the vascular system. Among auxin carriers, AUX1 is involved in LR initiation and LAX3 in LR emergence (Marchant et al., 1999, 2002). AtHB23 regulates *LAX3*, whereas AtMYB68 modulates *AUX1* expression in primary roots and LRs.

The three TFs are induced in salinity conditions exerting cooperative (AtHB23 and AtMYB68) and opposite (AtPHL1) functions (Figure 5). Like *amiR23*, *amiR68* and ATPHL1 plants showed a reduced survival capacity in 150 mM NaCl, accompanied by a lower ability to elongate primary roots exploring a less saline medium. Regarding LR elongation, *amiR68* plants were less penalized in NaCl than in control conditions, whereas *phl1* mutants lost their more elongated phenotype.

Under abiotic stress conditions, the survival ability was correlated with the conservation or degradation of amyloplasts in the columella cells (Takahashi et al., 2003). Notably, LRs enter salinity conditions that are lethal for the primary root (Ambastha et al., 2020). *AtHB23* silencing provoked the loss of starch granules (Perotti et al., 2022). After analyzing amyloplasts in single mutants and crosses, we propose that since AtHB23 is necessary to deal with salinity and silenced plants cannot survive in such conditions, the action of this gene is fine-tuned. The phenotype of the crosses under salinity conditions supported this interpretation (Figure 6). AtMYB68 interaction is required for this

function, and AtPHL1 kidnaps both TFs by protein–protein interactions to modulate such response (Figure 7).

Altogether, our results indicate a fine regulation of primary root and LR development in normal growth and in salinity conditions by the interplay between AtHB23, AtMYB68, and AtPHL1 (Figure 7).

EXPERIMENTAL PROCEDURES

Plant material and growth conditions

Arabidopsis thaliana plants (accession Col-0) were grown on Klasmann Substrate N° 1 compost (Klasmann-Deilmann GmbH, Germany) in a growth chamber at 22–24°C under long-day (16/8 h light/dark cycles) conditions, with a light intensity of approximately 120 µmol m^{-2} sec^{-1} in 8 × 7 cm pots. Four plants were planted per pot unless stated otherwise.

Transgenic plants carrying *AUX/LAX* promoters fused to *GUS*, which were previously described (*prAUX1:GUS*: Marchant et al., 1999, 2002; *prLAX1:GUS*: Bainbridge et al., 2008; and *prLAX3:GUS*: Swarup et al., 2008), were generously gifted by Dr. Swarup's lab.

Arabidopsis mutant lines *phl1*-1 and -2 (SAIL_731_B09) and (SALK_079505.20.10) and *DR5:GFP* transgenic plants were obtained from the Arabidopsis Biological Resource Center (ABRC) stock. *AtHB23* silenced plants (*amiR23*), *prAtPHL1:GUS*, *prAtHB23$_L$:GUS*, and *prAtHB23$_S$:GUS* were previously described (Perotti et al., 2019; Perotti et al., 2022; Spies et al., 2022).

Genetic constructs used for plant transformation

35S:AtMYB68: The vector *pENTER223* harboring the coding sequence of *AtMYB68* (G22683) was purchased and the *AtMYB68* sequence was recombined into the *pFK247* plasmid using the Gateway® (Invitrogen, Carlsbad, CA, USA) system.

35S:AtMYB68:GFP: Using as probe the construct *pENTER223-AtMYB68* (see above), the *AtMYB68* coding sequence was amplified with specific oligonucleotides (Table S1). The amplification product was introduced in the *pGEM T-easy* vector and then subcloned in the plasmid *pENTER3C* between the *Bam*HI and *Xba*I sites. By Gateway® (Invitrogen) recombination, it was finally cloned in the destination vector *pFK248*.

35S:amiR68: The design of amiRMYB68 was carried out with WMD3 software (Web MicroRNA Designer; wmd3.weigelworld.org) (Schwab et al., 2006). Four oligonucleotides (Table S1), endogenous miR319a, and the binary vector *pNB47* were used in an overlap PCR. The amplification product was cloned in the *pGEM T-easy* vector and then in the *pENTER3C* previously digested with *Bam*HI and *Eco*RI. Finally, amiRMYB68 was introduced in the *pKGWFS7* destination plasmid using the Gateway® (Invitrogen) recombination system.

PrMYB68:GUS:GFP: A 2377-bp fragment upstream of the ATG codon corresponding to the promoter region of *AtMYB68* was amplified by PCR using genomic DNA and specific oligonucleotides (Table S1). The PCR product was cloned into the *pGEM-T easy* vector, digested with *Bam*HI and *Xho*I, and finally recombined into the *pKGWFS7* destination plasmid using the Gateway® (Invitrogen) system.

Genetic constructs used for BiFC and colocalization analyses

For PCR, cDNA was used as a template. Primers are listed in Table S1.

AtHB23:GFP, ***Myc-AtHB23***, ***Venus-N:AtHB23***, and ***Venus-C:AtHB23***: A 765-bp fragment starting from the ATG codon (translation start site [TSS]) of the *AtHB23* gene was amplified with specific oligonucleotides (Table S1) and cloned into the pMDC83 (Ka+) Gateway® vector system (Invitrogen), the Myc-pBA vector harboring a fragment encoding an N-terminal 6×Myc tag, the pDEST-GWVYNE vector, and the pDEST-GWVYCE vector (GATEWAY-BiFC vectors; Gehl et al., 2009).

MYB68:RFP, ***HA-AtMYB68***, ***Myc-AtMYB68***, ***Venus-N:AtMYB68***, and ***Venus-C:AtMYB68***: A 1122-bp fragment starting from the ATG codon (TSS) of the *AtMYB68* gene was amplified by PCR using cDNA and specific primers (Table S1). The PCR product was cloned into the pH7RWG2 (Spec+) Gateway® vector system (VIB-UGent Center for Plant Systems Biology), the HA-pBA vector harboring a fragment encoding an N-terminal 3×HA tag, and the HA-pBA vector, the pDEST-^{GW}VYNE, and pDEST-^{GW}VYCE vectors.

HA-AtPHL1, ***Venus-C:AtPHL1***, and ***Venus-N:PHL1***: A 1239-bp fragment starting from the ATG codon (TSS) of the *AtPHL1* gene was amplified by PCR and cloned into the HA-pBA vector, the pDEST-^{GW}VYCE vector, and the pDEST-^{GW}VYNE (Ka^+) vector.

NLS-RFP: The plasmid harboring a nuclear localization signal (NLS)-tagged RFP gene (*NLS-RFP*) was obtained from Prof. Sang Yeol Lee's lab (Gyeongsang National University, Jinju).

Venus-N:AtHY5: A 540-bp fragment starting from the ATG codon (TSS) of the *AtHY5* gene was amplified and cloned into the pDEST-^{GW}VYNE vector.

Venus-C:AtSTO: A 744-bp fragment starting from the ATG codon (TSS) of the *AtSTO* gene was amplified by PCR and cloned into the pDEST- vector.

AD:PHL1, ***BD:PHL1***, ***AD:AtHB23ΔAHA***, and ***BD:AtHB23ΔAHA***, which were used for Y2H assays, were previously described (Spies et al., 2022).

Arabidopsis stable transformation

Stable transformation of Arabidopsis plants was performed via a floral dip procedure as previously described (Clough & Bent, 1998). *Agrobacterium tumefaciens* strain LBA4404 carrying the constructs described below was used for transformation. Selection was performed on the basis of their resistance to Basta (50 mg L^{-1}) or kanamycin (50 mg L^{-1}).

Transgene insertions were verified by PCR using genomic DNA as a template and specific oligonucleotides (Table S1). Three/four positive independent lines were further reproduced and homozygous T3 and T4 plants were used for further analyses.

Plant crosses

Mutant plants *phl1-1*, *phl1-2*, *amiR68-1*, and *amiR68-5* were fertilized with pollen from *prAUX1:GUS*, *prLAX1:GUS*, and *DR5:GUS* genotypes and then selected based on their resistance to the corresponding chemical, depending on the donor (kanamycin resistance for the constructs bearing the promoters of *LAX1* and *AUX1*).

AmiR23 and AT23 plants were fertilized with pollen from *phl1-1*, *phl1-2*, *OEPHL1-14*, *OEPHL1-16*, *amiR68-1*, and *amiR68-5* genotypes, whereas AT68-5 plants were fertilized with pollen from *amiR68-1* and *amiR68-5* genotypes.

Yeast two-hybrid screening

A truncated version of AtHB23 (AtHB23ΔAHA; Capella et al., 2014) was used as bait for Y2H screening as previously described (Spies et al., 2022).

Transient transformation of *N. benthamiana* for colocalization and BiFC analyses

Nicotiana benthamiana leaves were transformed by infiltration with a syringe containing 10 mM MES, 0.1 mM acetosyringone, 10 mM $MgCl_2$, and cultured *A. tumefaciens* GV3101 (at an OD_{600} of 0.3) previously transformed with the constructs indicated in the corresponding figures and mixed with *A. tumefaciens* cells transformed with the silencing inhibitor p19. Two days after infiltration, samples were harvested starting 2 h before the end of the day and used for visualization under a confocal microscope (FLUOVIEW FV3000 Olympus confocal laser microscope). Samples were excited using a 514-nm laser, and emission was detected using two channels: 520–530 nm for Venus and 540–600 nm for lignin autofluorescence.

Coimmunoprecipitation

Nicotiana benthamiana leaves were infiltrated with *A. tumefaciens* GV3101 at a final OD_{600} of 0.5. Proteins were extracted using a buffer containing 100 mM Tris–HCl (pH 7.4), 150 mM NaCl, 1 mM EDTA (pH 8.0), 0.1% NP40, and protease inhibitor cocktail (5 μg ml^{-1} Leupeptin, 1 μg ml^{-1} Aprotinin, 5 μg ml^{-1} Antipain, 1 μg ml^{-1} Pepstatin A, 5 μg ml^{-1} Chymostatin, 3 mM DTT, 100 μM PMSF, 1.5 mM Na_3VO_4, 2 mM NaF, and 50 μM MG132), and coimmunoprecipitated using the Dynabeads™ Protein A Immunoprecipitation Kit (Invitrogen™, Catalog No. 10006D) with mouse monoclonal anti-Myc tag (9B11, Cell Signaling Technology®, Catalog No. 2276S). Proteins were separated by 10% SDS-PAGE and transferred to Immobilon®-P PVDF membranes (Merck Millipore Ltd., Catalog No. IPVH00010) using a Trans-Blot® Turbo™ Transfer System (Bio-Rad, Catalog No. #1704150). The proteins were detected by incubating the membranes with horseradish peroxidase (HRP)-conjugated anti-HA (Roche, product code: 12013819001) and HRP-conjugated mouse monoclonal anti-Myc tag (9B11, Cell Signaling Technology®, Catalog No. 2040S) for 2 h at room temperature. Images were taken using a ChemiDoc™ MP Imaging System (Bio-Rad, Catalog No. 12003154).

Root phenotyping

For root phenotyping, seeds (Col-0, mutant, and overexpressor plants) were surface sterilized and placed at 1 cm from the top of square Petri dishes (12 × 12 cm) for 3 days at 4°C before placing the dishes in the growth chamber at 22–24°C for five additional days under long-day (16/8 light/dark cycle) conditions with a light intensity of approximately 110–120 μmol m^{-2} sec^{-1}. The growth medium was Murashige–Skoog medium supplemented with vitamins (MS, PhytoTechnology Laboratories™).

For root surveys, photograph series were taken and analyzed with ImageJ and RootNav software.

Salinity and osmotic stress treatments

Seedlings were grown in normal conditions as described above and then placed in plates with the same medium supplemented with NaCl (concentrations indicated in the corresponding figure legends). Primary roots were analyzed after an additional 5 days of growth when seedlings were 8 days old. To analyze the kinetics of primary root elongation, root length was measured every 2 days until day 10.

The survival experiment was performed with plants placed in 100 mM NaCl after 3 days of growth in normal conditions. The counting was done on different days as indicated in the corresponding figure legend.

For amyloplast observation, 5-day-old plants grown in control conditions were treated for 8 h with 150 mM NaCl. After that, half of the plants were transferred to control conditions and the other half remained in the saline medium for an additional 72 h. Osmotic treatments were carried out essentially as described above but with 150 mM mannitol instead of 150 mM NaCl.

GUS histochemistry

In situ assays of GUS activity were performed essentially as described by Jefferson et al. (1987) with little modifications (Ribone et al., 2015).

RNA isolation and expression analyses by RT-qPCR

Total RNA was isolated for real-time RT-PCR analysis from rosette leaves of 25-day-old plants or 5–8-day-old roots using TRIzol® reagent (Invitrogen) according to the manufacturer's instructions. Total RNA (1 μg) was reverse-transcribed using oligo$(dT)_{18}$ and M-MLV reverse transcriptase II (Promega, Fitchburg, WI, USA).

qPCR was performed using an Mx3000P Multiplex qPCR system (Stratagene, La Jolla, CA, USA) as described before (Mora et al., 2022) using the primers listed in Table S1. Transcript levels were normalized by applying the $2^{-\Delta\Delta Ct}$ method. Actin transcripts (*ACTIN2* and *ACTIN8*) were used as internal standards. Three biological replicates, obtained from three individual plants and tested in duplicate, were used to calculate the standard deviation.

Amyloplast staining and light microscopy observation

To observe the amyloplasts in the columella cells of the root tips, 15–20 5-day-old Arabidopsis roots were dipped in Lugol staining solution (Sigma-Aldrich) for 8–10 min, washed with distilled water, and then observed using an Eclipse E200 Microscope (Nikon, Tokyo, Japan, https://www.nikon.com/) equipped with a Nikon Coolpix L810 camera.

For salinity or osmotic treatments, seedlings were transferred to Petri dishes with MS medium supplemented with 150 mM NaCl or 150 mM mannitol for 7–8 additional hours, according to the method described by Sun et al. (2008).

Fluorescence microscopy

For confocal imaging, roots from different genotypes were treated with 10 μg ml^{-1} propidium iodide, rinsed with a drop of distilled water, and examined and imaged using a confocal inverted microscope (Confocal LEICA TCS SP8) with a 20× objective. Propidium iodide was excited using a 514-nm line laser (18% intensity), and emission was detected at 498–532 nm using bandpass filters.

Statistical analysis

Phenotypic characteristics such as primary root length, total LR length, number of initiated and emerged secondary roots, and number of cells, as well as qPCR data, were statistically analyzed using one-way analysis of variance (ANOVA) considering genotype as the main factor.

Significant differences between means were analyzed using Tukey's post hoc comparison and are indicated by different letters. The number of biological replicates for each assessment is indicated in the corresponding figures.

ACCESSION NUMBERS

Genes can be found with the following accession numbers: AT1G26960 (*AtHB23*), AT5G65790 (*AtMYB68*), AT5gG29000